Considerations on External Heat Transfer in Saturated Bipolar Junction Transistors

Riccardo Carotenuto, *Senior Member, IEEE*, Demetrio Iero, Fortunato Pezzimenti, Francesco G. Della Corte, *Senior Member, IEEE*, and Massimo Merenda, *Member, IEEE*

***Abstract*— When the BJT is deeply saturated and a resistor (R) is connected between the base and collector, the overall bipole seen through the base and emitter exhibits rectifying properties. By appropriately sizing R, only a small fraction of the current flows into the base, while the majority passes through R, causing a voltage drop almost equal to that between the base and emitter. The same current flows through the collector and emitter, resulting in a voltage drop on the order of tens of millivolts. The novelty lies in the fact that almost all the power is dissipated in R rather than in the BJT. In the presence of large currents, this leads to significantly lower power dissipation in the BJT compared to a diode of the same size. The reduced thermal stress can extend the mean time between failures (MTBFs) of the BJT. In this study, we conduct a model-based analysis of the saturated BJT rectifier, which is then validated through experimental setups. Furthermore, it is demonstrated that the power dissipated in a saturated BJT-based bridge rectifier is significantly lower than that measured in a classical bridge rectifier configuration under the same operating conditions.**

***Index Terms*— BJT heating, BJT heat transfer, BJT physical effect, BJT saturation.**

I. Introduction

CURRENT rectification is a crucial nonlinear operation in signal and power applications. In power applications, electrical power is converted from alternating to direct current [1], [2], [3], [4], [5]. Current rectification power levels in state-of-the-art applications range from a few milliwatts in consumer electronics to hundreds of kilowatts, for example, in inverter-type air conditioners, and more recently, in electric vehicle charging circuits [6], [7], [8], [9], [10], [11], [12]. Traditionally, silicon or silicon carbide diodes have been dedicated to passive current rectification in well-known diode bridge schemes. Passive schemes have an advantage over more sophisticated active rectifiers based, for example, on MOSFET bridges, as they are simpler, cheaper, and less prone to failures. Considering the stress at the device level and its related reliability, passive schemes provide lower values of the failure rate, and consequently, higher values of mean time between failure (MTBF), which is a parameter of primary importance in safety-related application fields such as renewable energy, space, automotive and railways [13], [14], [15]. In fact, the MTBF of a semiconductor device, and consequently its duration, increases considerably as the actual operating temperature decreases, according to the MTBF equation, derived from the well-known Arrhenius equation, which relates temperature and lifetime.

Although diode circuits work satisfactorily for low-power applications, as the power level increases efficiency and power dissipation issues become increasingly crucial. The voltage drop on the diodes crossed by hundreds of amperes, as in the case of the charging circuits of electric vehicles, causes a significant loss of electrical power which is converted into heat. Consequently, the current rectification circuits overheat and the temperature can rise to dangerous levels, eventually destroying the devices. External cooling devices are usually adopted to mitigate and control overheating, including fins, forced air coolers, and liquid coolers [16]. However, this increases the size and cost of the current rectifiers.

The bipolar junction transistor [17], [18], invented in the late 1940s, has revolutionized the nascent field of electronics. BJT has made it possible to realize sophisticated amplifiers for linear amplification of very weak analog signals, source-load impedance matching, power amplification up to kilowatts, and bandwidth spanning from direct current to microwaves. BJT was also the core of the first logical circuits [resistor transistor logic (RTL), transistor-transistor-logic (TTL)] that laid the foundations of the modern digital revolution. In recent years, considerable efforts have been made to model BJTs and optimize their performance for each intended application. Many effects have been discovered in the various operating conditions, such as the early effect or the high injection effect, just to name a few.

In this work, a phenomenon of "side" heat exchange that has so far remained unnoticed, which however becomes macroscopic only when a BJT is biased in its direct saturation region is exploited to build a new current rectification circuit with reduced heat release.

A basic rectification circuit showing an unconventional BJT biasing scheme was presented and compared with two other traditional schemes. In the novel circuit, the BJT working in its

Manuscript received 8 March 2024; revised 6 June 2024; accepted 14 June 2024. Date of publication 21 June 2024; date of current version 2 August 2024. Recommended for publication by Associate Editor Lin Liang. *(Corresponding author: Riccardo Carotenuto.)*

Riccardo Carotenuto and Fortunato Pezzimenti are with the Dipartimento di Ingegneria dell'Informazione, delle Infrastrutture e dell'Energia Sostenibile (DIIES), Università Mediterranea di Reggio Calabria, 89122 Reggio Calabria, Italy (e-mail: r.carotenuto@unirc.it; fortunato.pezzimenti@unirc.it).

Demetrio Iero and Massimo Merenda are with the Dipartimento di Ingegneria dell'Informazione, delle Infrastrutture e dell'Energia Sostenibile (DIIES), Università Mediterranea di Reggio Calabria, 89122 Reggio Calabria, Italy, and also with HWA srl, 89122 Reggio Calabria, Italy (e-mail: demetrio.iero@unirc.it; massimo.merenda@unirc.it).

Francesco G. Della Corte is with the Dipartimento di Ingegneria Elettrica e delle Tecnologie dell'Informazione (DIETI), Università di Napoli Federico II, 80125 Naples, Italy, and also with HWA srl, 89122 Reggio Calabria, Italy (e-mail: francescogiuseppe.dellacorte@unina.it).

Color versions of one or more figures in this article are available at https://doi.org/10.1109/JESTPE.2024.3417526.

Digital Object Identifier 10.1109/JESTPE.2024.3417526

saturation region exhibits reduced dissipated power compared to the other schemes. More complex or optimized circuits could be proposed to exploit this phenomenon; however, the main purpose of this study is to show the existence of the phenomenon, namely the heat transfer from the saturated BJT to the external resistor, which, to the best of our knowledge, has not been reported in the literature.

Sections II and III describe the operating principle, propose a physical explanation, describe the experimental setups, and discuss experimental results. Finally, Section IV presents the conclusions of this study.

II. Operating Principle and Physical Insight

A bipolar junction transistor is composed of three properly doped semiconductor regions: collector, base, and emitter [19], [20]. Owing to the different concentrations of dopants, potential barriers are created at the emitter-base junction (EBJ) and the collector-base junction (CBJ), balancing the opposite diffusion and drift currents. BJT can be of two types, NPN and PNP, according to the dopant patterns. Let us consider an NPN BJT without a loss of generality. The same reasoning applies to the PNP BJT in a straightforward manner. Fig. 1 represents a longitudinal section of an ideal NPN BJT, and for simplicity, only the majority carriers, that is the electrons, are represented. Furthermore, potential barriers are observed for the electrons. Bipolar transistors have four distinct regions of operation defined by the bias condition of each BJT junction.

In the NPN transistor, the EBJ electrical field E_{EBJ} is directed from the emitter to the base, whereas the CBJ electrical field E_{CBJ} is directed from the collector to the base. Fig. 1 also shows the simplified force vectors $F_{\mathrm{EBJ}} = -qE_{\mathrm{EBJ}}$ and $F_{\mathrm{CBJ}} = -qE_{\mathrm{CBJ}}$ acting on the electrons, where $-q$ is the electron charge. When a forward voltage bias is applied between the base and emitter terminals, the potential barrier at EBJ is lowered by approximately the same amount and free electrons, which are abundant in the emitter region, can overcome the EBJ barrier and diffuse into the base region [see Fig. 1(b)].

These electrons are continuously replaced by new ones coming from the external circuit through the ohmic contact of the emitter, almost to form the total current I_E, without considering the other minor contributions such as the holes injected from the base. The electrons diffuse in the typically narrow base regions toward CBJ, but in part recombine with the relatively abundant base holes, and in a small fraction reach the base ohmic contact, originating, in part, the relatively small current I_B.

In the forward active region, the collector-base terminals are reverse-biased, which increases the CBJ potential barrier. After traveling across the base region, the electrons coming from the emitter reach the depletion region of the CBJ. Here, the electrons are swept by the electric field down to the collector region and through the collector ohmic contact, flowing out of the BJT into the external circuit and generating the collector current I_C.

The entire process can also be viewed from a thermodynamic perspective. Here, for simplicity, but without loss of generality, this reasoning is limited to the majority charge carriers, in this case, electrons. Statistically, electrons accelerate down the slope of the CBJ potential barrier, acquire kinetic energy thus increasing their temperature, proportional to the height of the barrier, and then release a certain amount of heat into the collector region. On the other hand, at EBJ, only the most energetic or hot electrons can overcome the potential barrier traveling from the emitter into the base. While leaving the emitter region, they lower the local average temperature of the carriers, and thus of the entire emitter region, as occurs similarly in liquids, where evaporation cools down the remaining liquid, neglecting the heat absorption of the liquid-gas molecular transition. In the forward active operations of the BJT [see Fig. 1(b)], the height at the EBJ of the barrier is much lower than that at CBJ, and the cooling effect at the EBJ is much smaller than that at CBJ.

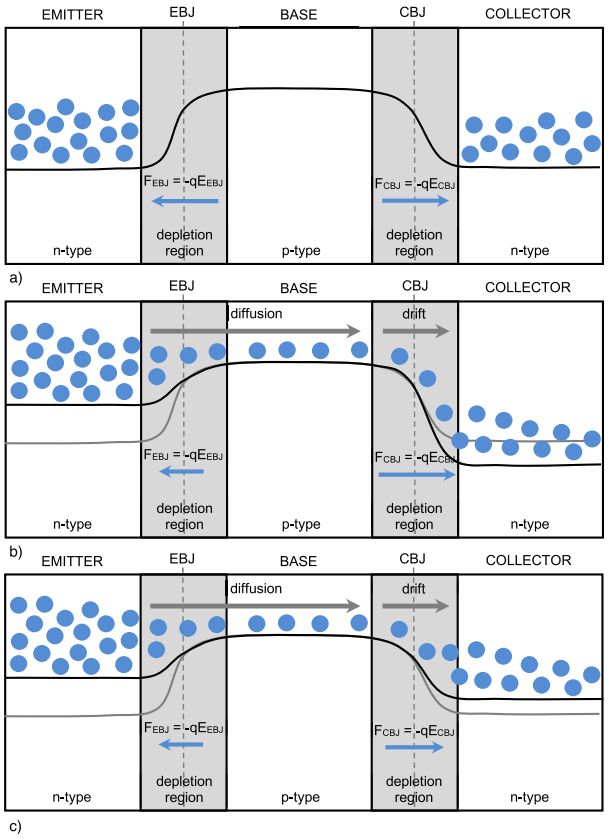

Fig. 1. Simplified pictorial view of the internal structure, electrons, and internal potential diagram for electrons for an NPN BJT. The represented potential diagram holds for negative charges, i.e., for electrons (light blue dots). Minority carriers, recombination, and width modulation of depletion regions with biasing are not shown. (a) Without external bias: electron concentration and potential distribution at equilibrium, when the drift and diffusion currents, opposite each other, are perfectly balanced. (b) Forward active region. (c) Forward saturation region. F_{EBJ} and F_{CBJ} are the forces with different magnitudes and directions acting on each electron due to the electric fields E_{EBJ} and E_{CBJ} in the depletion regions (not in scale). Note that the free electrons concentration in the emitter is made higher than that in the collector by design.

A thorough analytical and experimental discussion of heat exchange in semiconductor devices can be found in [21], [22], and [23], where it is shown that when charge carriers encounter internal potential variations along their path in a semiconductor, there is always heat exchange, that is heat

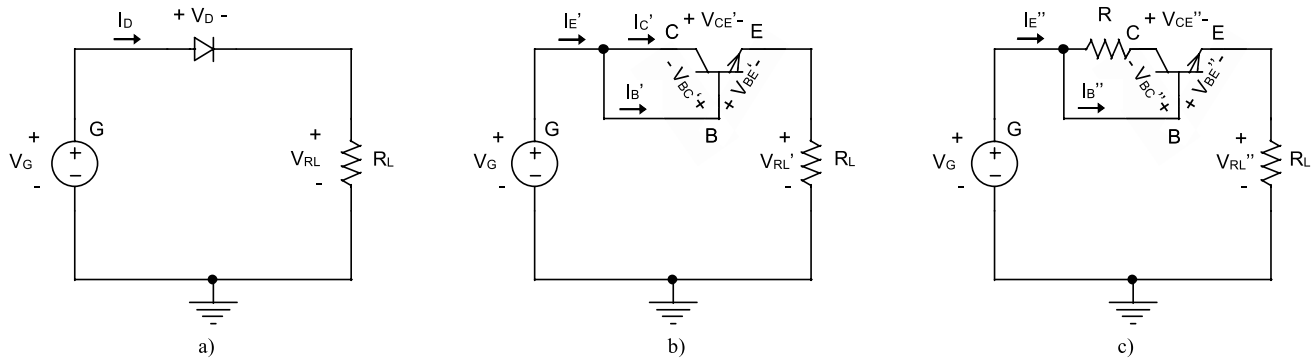

Fig. 2. Rectification circuits (a) basic diode rectifier, (b) diode-connected BJT rectifier, and (c) saturated BJT rectifier.

release, when charge carriers move from regions with high potential to regions at low potential and heat absorption in the opposite case. For example, in semiconductors, the loss of potential and related heating occurs with electron-hole recombination processes and lattice collisions in the crystal body.

A. Basic Current Rectifiers Power Balance

To show the presence of a noticeable heat exchange inside the saturated BJT, the power balance of three basic current rectification circuits is calculated, considering static voltages and currents for simplicity, without loss of generality of the results. Today, many rectifier circuits are known to have a higher efficiency, such as synchronous rectifiers, which therefore, represent a superior class of circuits, but which unfortunately show reduced reliability and increased cost and size compared to simpler circuits. In this study, to focus on the physical phenomenon we are dealing with, we choose to compare our circuit with the most similar in terms of reliability, complexity, and size, namely, the diode rectifier. Furthermore, to avoid introducing unnecessary elements such as transient behaviors, we focus on a static example, that is with constant voltages and currents.

The first is a very popular circuit based on the diode, which is assumed to be made of silicon, while the other two use a silicon BJT as the rectifier element. In particular, the second circuit exploits the diode connection, which is widely used in integrated circuits in place of diodes.

Let us first consider the simple circuit shown in Fig. 2(a) consisting of a series of a voltage generator G of value V_G, which is considered constant and sufficient to conduct diode D, of a silicon diode D operating at voltage V_D^{ON} and of a load resistor R_L.

The power balance of the circuit in Fig. 2(a) is as follows:

$$P_G = V_G \cdot I_G \tag{1}$$
$$P_D = V_D^{\mathrm{ON}} \cdot I_D \tag{2}$$
$$P_{RL} = V_{RL} \cdot I_G = \left(V_G - V_D^{\mathrm{ON}}\right) \cdot I_D \tag{3}$$
$$P_G = P_D + P_{RL}. \tag{4}$$

As is known, P_D is the power lost in the diode during rectification, which lowers the efficiency of the circuit and causes the diode to heat. In high-power applications, P_D has values in the order of kilowatts, with a consequent need to adopt strategies, even considerably expensive, to dissipate P_D to keep the diode temperature in the safe range. Heat dissipation techniques include fins, forced air coolers, and liquid-cooled circuits.

Let us now consider the circuit in Fig. 2(b), composed of the series of the voltage generator G, with a positive value V_G sufficient to conduct the BJT, of the NPN BJT connected as a diode, that is with the base and collector connected together, and of the load resistor R_L.

Since $V_{BC} = 0$, due to the "diode" connection and the base–emitter junction being directly biased, then the BJT operates in its direct active region and $V'_{BE} = V_{BE}^{\mathrm{ON}}$, here assumed to belong approximately to the 0.7–0.8 V range. Owing to the diode connection, $V'_{CE} = V_{BE}^{\mathrm{ON}}$ also holds; therefore, the power balance of the circuit with BJT connected to the diode is

$$P'_G = V_G \cdot I'_G = V_G \cdot I'_E \tag{5}$$
$$P'_{\mathrm{BJT}} = V_{BE}^{\mathrm{ON}} \cdot I'_B + V_{CE} \cdot I'_C = V_{BE}^{\mathrm{ON}} \cdot I'_E \tag{6}$$
$$P'_{RL} = V'_{RL} \cdot I'_G = \left(V_G - V_{BE}^{\mathrm{ON}}\right) \cdot I'_E \tag{7}$$
$$P'_G = P'_{\mathrm{BJT}} + P'_{RL}. \tag{8}$$

The power dissipated in the BJT P'_{BJT} assumes a level close to that of the diode of the previous circuit in the hypothesis that the forward voltage V_D^{ON} has a value comparable with V_{BE}^{ON}. This circuit, like the previous one, requires further means to dissipate excess heat. Note that in many practical applications, V_G is much larger than V_D^{ON} and V_{BE}^{ON}, therefore, their difference becomes negligible.

Finally, let us consider the circuit in Fig. 2(c), a series of voltage generator G of positive value V_G, of the NPN BJT, with the base and collector connected together through the resistor R and the load resistor R_L.

The power supplied to the circuit by the voltage generator G is

$$P''_G = V_G \cdot I''_G = V_G \cdot I''_E. \tag{9}$$

P_G will be dissipated differently in the BJT, in R, and in R_L.

The power in R_L is

$$P''_{RL} = \left(V_G - V_{BE}^{\mathrm{SAT}}\right) \cdot I'_E \tag{10}$$

where V_{BE}^{SAT} is the voltage across BE terminals V''_{BE} in the saturation region.

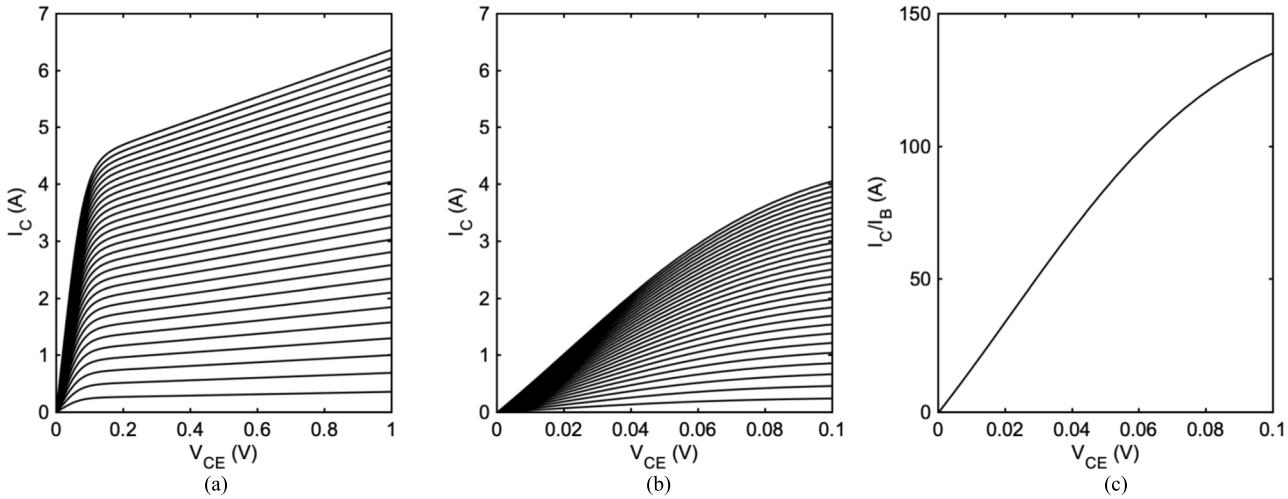

Fig. 3. Simulated transistor output curves using the NPN BJT 2SC6082 PSPICE model in the range from 0 to 1 V and for 30 equally spaced I_B current steps from 1 to 30 mA. (a) V_{CE} between 0 and 1 V, (b) zoomed portion of the output curves in the saturation region (0–0.1 V), and (c) current gain I_C/I_B in the saturation region. It can be noted that I_C is a multiple of I_B still in the deep saturation region (where V_{CE} has values in the range of tens of millivolts).

The power dissipated in R is

$$P_R = V''_{BC} \cdot I''_C = \left(V''_{BE} - V''_{CE}\right) \cdot I''_C = \left(V^{\mathrm{SAT}}_{BE} - V^{\mathrm{SAT}}_{CE}\right) \cdot I''_C \tag{11}$$

where $V''_{BC} = V'_{BE} - V''_{CE}$.

The power dissipated in the BJT is then

$$P''_{\mathrm{BJT}} = P''_G - P''_{RL} - P_R = V_G \cdot I''_E - \left(V_G - V^{\mathrm{SAT}}_{BE}\right) \cdot I''_E - \left(V^{\mathrm{SAT}}_{BE} - V^{\mathrm{SAT}}_{CE}\right) \cdot I''_C = V^{\mathrm{SAT}}_{BE} \cdot I''_B + V^{\mathrm{SAT}}_{CE} \cdot I''_C. \tag{12}$$

Comparing the circuits in Fig. 2(a) and (b), the power in R_L is almost the same

$$P'_{RL} = \left(V_G - V^{\mathrm{ON}}_{BE}\right) \cdot I'_E \approx \left(V_G - V^{\mathrm{SAT}}_{BE}\right) \cdot I''_E = P''_{RL} \tag{13}$$

under the realistic assumption that $I'_E \approx I''_E$ and that V^{SAT}_{BE} and V^{ON}_{BE} are both small compared with V_G.

However, with the reasonable assumptions that $I''_C > I''_B$ and that $V^{\mathrm{SAT}}_{CE} < V^{\mathrm{ON}}_{BE}$, the power P''_{BJT} in the saturated BJT is noticeably less than P'_{BJT} in the diode-connected BJT

$$P''_{\mathrm{BJT}} = V^{\mathrm{SAT}}_{BE} \cdot I''_B + V^{\mathrm{SAT}}_{CE} \cdot I''_C < V^{\mathrm{ON}}_{BE} \cdot I'_E = P'_{\mathrm{BJT}}. \tag{14}$$

In fact, $I''_C > I''_B$ still holds in a large part of the saturation region, as shown for example in the exemplary output curves in Fig. 3, obtained from the PSPICE model of silicon BJT 2SC6082-1E [24]. However, as can be easily verified, depending on the specific values of the voltages V^{SAT}_{BE}, V^{SAT}_{CE}, and V^{ON}_{BE}, (14) also holds for some $I''_C < I''_B$ values.

In summary, the body of the BJT is crossed by almost the same current magnitude in both the circuits of Fig. 2(b) and (c), but when the BJT works in its saturation region, the dissipated net power is less than the power dissipated in the diode-connected BJT [see Fig. 2(b)], and all other conditions are nearly the same.

Remarkably, the power dissipated in diode D can be considerably greater than that dissipated in the BJT in the configuration proposed in Fig. 2(c). In fact, from (2) $P_D = V^{\mathrm{ON}}_D \cdot I_D$, and from the first member of (14), $P''_{\mathrm{BJT}} = V^{\mathrm{SAT}}_{BE} \cdot I''_B + V^{\mathrm{SAT}}_{CE} \cdot I''_C$, so that it is obtained

$$P_D > P''_{\mathrm{BJT}} \tag{15}$$

where it is assumed that $V^{\mathrm{ON}}_D \approx V^{\mathrm{SAT}}_{BE}$, that $V^{\mathrm{SAT}}_{BE} < V^{\mathrm{SAT}}_{CE}$, because both devices are built with the same silicon technology, $I_D \approx I_E$ because V_G (which is $\gg V^{\mathrm{ON}}_D$) and R_L are the same in all the circuits, and $I''_C > I''_B$. In particular, (15) is the more true, the more $I''_C > I''_B$.

From what has just been seen, it is therefore possible to conceive a current rectification circuit using a saturated BJT, which has a dissipated power in the active device that can be considerably lower than that dissipated in the diode, all other conditions being the same. The excess power is dissipated in the external resistor R which, in contrast to silicon devices, can be made with suitable techniques and materials that are very resistant to heat and able to withstand much higher temperatures. Resistor R can be placed at a certain distance from the BJT to avoid proximity overheating. On the other hand, unfortunately, no advantage is obtained from the new circuit in terms of overall performance, which remains practically unchanged.

It should also be noted that BJTs are commonly designed to operate in their direct active regions, with a high current gain. In saturation, on the other hand, the actual available current [see Fig. 3(b)] is much lower than that available in the direct active region. Therefore, for practical use, it will be necessary to provide an appropriate BJT design, especially with regard to its internal geometry and doping profiles, dedicated to optimizing the saturation performance.

B. Physical Insights

From a physical perspective, the difference in power dissipated in the two configurations presented above can be explained by considering the bias of the CBJ and EBJ junctions in the two cases. In Fig. 1(b) and (c), it can be seen the only significant difference is the potential barrier height at the CBJ junction.

TABLE I
EXPERIMENTAL SETUP

Circuit	V_G (V)	Device	R_L (Ω)	R (Ω)
Diode (Fig. 1a)	31.6	VS-20ETS16THM3	100	-
Diode-connected *BJT* (Fig. 1b)	31.6	2SC6082-1E	100	-
Saturated *BJT* (Fig. 1c)	31.6	2SC6082-1E	100	2.2

TABLE II
EXPERIMENTAL RESULTS-PEAK VALUES

Circuit	P_G (W)	V_D, V_{BE} (V)	V_{CE} (V)	I_B (mA)	I_C (mA)	I_G (mA)	P_D, P_{BJT} (mW)	P_R (mW)	P_{RL} (W)	η
Diode	9.748	0.752	-	-	-	308.5	231.9	-	9.516	0.976
Diode-connected *BJT*	9.781	0.645	0.645	-	-	309.5	199.7	-	9.582	0.979
Saturated *BJT*	9.765	0.696	0.027	7.2	301.7	309.0	13.2	200.4	9.550	0.978

In fact, in the active region, as clearly visible in Fig. 1(b), the CBJ barrier is higher than the EBJ barrier, and thus the heat released and absorbed do not compensate for each other. Therefore, by using the diode connection, which causes the BJT to work in the active region, the heat release is appreciably greater than the cooling, which results in a greater net heating of the device. In contrast, in the saturation region [see Fig. 1(c)] the height of the barrier of CBJ is approximately the same as that of EBJ, therefore, the quantities of heat released and adsorbed are approximately the same with a much smaller net released heat.

III. EXPERIMENTAL SETUPS AND MEASUREMENT RESULTS

In this section, a first experimental setup is presented to demonstrate the validity of the above considerations without the intent of providing a real application example or providing a comparison with consolidated rectifiers based on synchronized transistors. The sizing of the maximum voltage and power was carried out by considering silicon devices that are easily available on the market. The experimental setup is described and characterized with reference to the circuits shown in Fig. 2. Table I summarizes the components used, and Table II reports the experimental results. Note also that all experimental values were obtained at the peak value, thus eliminating the unnecessary complication of the dynamic behavior of the components in the present context. A second experiment, consisting of a 230 V_{RMS}, 50 Hz bridge rectifier with a power rating of about 445 W, was built and characterized to verify the dynamic behavior under a realistic power level.

A. Experimental Setup I: DC Working Principle Investigation

The three circuits under investigation are sized to work for power with a peak just under 10 W with a voltage source of peak amplitude $V_G = 31.6$ V and $R_L = 100$ Ω. The circuit shown in Fig. 2(a) was realized using the diode VS-20ETS16THM3 [25]. The circuit shown in Fig. 2(b) is made with a diode-connected BJT 2SC6082-1E. The circuit in Fig. 2(c) is made with the same BJT and a resistor R of value 2.2 Ω. This resistor value was selected by minimizing the power dissipated in the BJT using the PSPICE model of the 2SC6082-1E BJT and the PSPICE goal function analysis. However, as a rule of thumb, a closely approximate value of R can be calculated imposing $V_{CE} \approx 0$ (i.e., a very deep BJT saturation) in the circuit of Fig. 2(c). From the R and BC voltage loop

$$I_C'' \cdot R = V_{BE}^{\mathrm{SAT}} \tag{16}$$

and from the main voltage loop

$$I_C'' = \left(V_G - V_{BE}^{\mathrm{SAT}}\right)/R_L. \tag{17}$$

Finally, combining (16) and (17), the following approximate formula is obtained:

$$R \approx V_{BE}^{\mathrm{SAT}} \cdot R_L/\left(V_G - V_{BE}^{\mathrm{SAT}}\right). \tag{18}$$

The same PSPICE model was used to obtain the BJT output curves of Fig. 3, considering the input voltage constant and equal to the peak value $V_G = 31.6$ V and $R_L = 100$ Ω. Table I summarizes the values of the components used in each circuit.

An image of the three realized circuits is shown in Fig. 4(a)–(c). The circuits in Fig. 4 are complete rectifier bridges with four diodes and four BJTs; only one branch realizes the circuits shown in Fig. 2. The following measurements were performed considering only one of the four branches of the complete bridge. A 100 Ω resistor (not shown in Fig. 4) with a tolerance of 1% was used as a load, capable of dissipating 10 W without requiring any additional heat sink.

The voltage source was a GW-Instek GPS3303 and the currents and voltages were measured using Agilent U1272A.

B. Experimental Setup I: Results

The experiment consists of estimating the power dissipated in the active components in the three configurations from the measured current and voltages. As anticipated, to highlight the physical phenomenon under examination, the dynamic phenomena, normally present in the rectification cycle, were avoided by applying a direct voltage equal to the peak input voltage. Therefore, all measured voltages and currents and estimated powers are peak values. The results are summarized in Table II which reports the power P_G supplied to the circuit by the voltage source G, the voltage measured across the

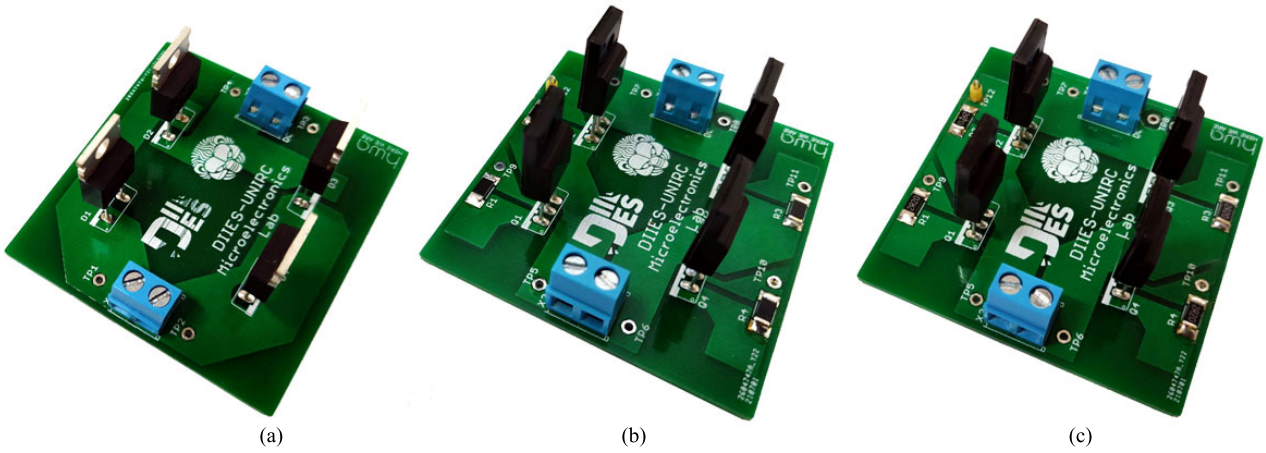

(a) (b) (c)

Fig. 4. Realized rectification circuits (a) basic diode rectifier, (b) diode-connected BJT rectifier, and (c) saturated BJT rectifier.

diode or *BE* terminals of the BJT, the voltage across the *CE* terminals, the base current I_B, the collector current I_C, and the current flowing through the voltage source G, which is the same as I_E and I_D, the estimated total power on the diode or BJT, R, and R_L for the three circuit configurations in Fig. 2. In detail, P_G is computed as $V_G \cdot I_E$ or $V_G \cdot I_D$, $P_D = V_D \cdot I_D$, $P_R = I_C^2 \cdot R$, $P_{RL} = V_{BE} \cdot I_B + V_{CE} \cdot I_C$, and the static efficiency η is estimated as the ratio P_{RL}/P_G. At the operating point, a β^{SAT} of approximately 41.9 was estimated for the saturated BJT configuration.

C. Experimental Setup I: Discussion

The voltage drop from voltage source G to the load R_L in the three circuits is small with respect to the value of V_G, here 31.6 V. Therefore, as reported in Table II, the power extracted from G and dissipated in R_L is about the same in all the three circuits. Moreover, the circuit efficiency η was approximately the same for the three circuits.

Therefore, the only substantial difference between the three circuits was the power dissipated in the active elements. It is important to note that the merit figure or performance of interest in this work is the power dissipated in the semiconductor-rectifying device, which is a characteristic that distinguishes the circuit proposed by the classic diode rectifier. In fact, the experimental results show that the peak power dissipated in the diode or diode-connected BJT, 231.9 and 199.7 mW, respectively, are significantly greater than those dissipated in the saturated BJT of the proposed circuit (13.2 mW). Indeed, it was experimentally observed that the ratio between the power dissipated in the diode and that dissipated in the BJT of the proposed circuit exceeded 17. This corresponds to a considerable BJT thermal stress reduction in the proposed circuit with respect to the diode and the diode-connected BJT, with the same boundary conditions. The observed total power dissipated in the proposed circuit is approximately 213.6 mW, which is very similar to that of the other circuits and is halfway between the power dissipated in the diode and the diode-connected BJT.

It was also experimentally confirmed that almost all the difference in the power dissipated in the BJT in the two configurations was dissipated in the external resistor R (i.e., 200.4 mW). Therefore, it can be concluded that the power dissipated in the diode-connected BJT in Fig. 2(b) is largely transferred to the external resistor R in the newly proposed circuit configuration in Fig. 2(c).

At this point, it is important to note that the resistor R can be made using a technology capable of withstanding high dissipated powers, such as using metal wires or sheets, without the need for further devices or dissipative means, and also that it can be placed at a convenient distance in such a way as to easily dissipate heat without warming up the BJT. Finally, it is evident that the BJT of the proposed circuit undergoes lower thermal stress, owing to the reduced dissipated power, and that it will have a considerably longer expected operating life. The presented experimental setup only served to demonstrate that in the new circuit based on a saturated BJT, the peak power dissipated in this BJT is lower than that dissipated in the diode or on a diode-connected BJT and that the power difference is dissipated in resistor R.

As previously mentioned, the load current of the proposed example (approximately 309 mA) is much less than the maximum current that the used BJT 2SC6082-1E can supply in its direct active region, which is approximately 15 A [24]. Therefore, while the presented experimental setup served to demonstrate the proposed operating principle by using off-the-shelf components, certainly, for real-world use, it is reasonable to think about designing a dedicated BJT from scratch.

The presented experimental setup only served to demonstrate that in the new circuit based on a saturated BJT, the peak power dissipated in the BJT is lower than that dissipated in the diode or a diode-connected BJT, and that the power difference is dissipated in resistor R. However, R has been sized here for a given value of R_L and V_G. It is evident that in real use, R must be sized to minimize the power dissipated in the BJT over the entire input voltage V_G cycle and for the expected range of R_L values.

In the proposed schemes, considering the full wave of input voltage, the active element supports an inverse peak voltage with negative values down to $-V_G$ during the negative cycle. While power diodes are built to withstand high reverse voltages, in general, this is not true for the *BE* junction, which is usually sized for a reverse bias of a few volts. It may be

TABLE III
EXPERIMENTAL RESULTS WITH THE ROLES OF EMITTER AND COLLECTOR REVERSED-PEAK VALUES

Circuit	P_G (W)	V_{BC} (V)	V_{CE} (V)	I_B (mA)	I_E (mA)	I_G, I_G (mA)	P_D, P_{BJT} (mW)	P_R (mW)	P_{RL} (W)	η
Fig. 5	9.811	0.6930	-0.027	18.9	-290.2	309.1	21.2	185.2	9.552	0.978

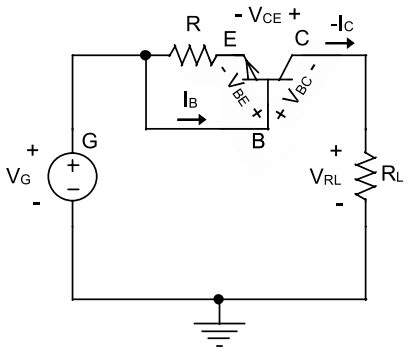

Fig. 5. Saturated BJT rectifier with C and E exchanged.

necessary to redesign the geometry and doping profiles of the BJT to support this new configuration. On the other hand, however, off-the-shelf parts might still be adequate. For example, the same BJT 2SC6082-1E can be profitably used in the proposed circuit simply by exchanging the roles of the emitter and collector (see Fig. 5). In fact, BJT 2SC6082-1E has a good value of β_{REVERSE} and supports an adequate reverse voltage at the base–collector junction ($V_{\text{CBO}} = 60$ V) [24]. This reasoning is supported by the experimental results presented in Table III. At the operating point, a $\beta^{\text{SAT}}_{\text{REVERSE}}$ of approximately 15 was experimentally determined.

Finally, it is interesting to note that in principle, through a suitable additional power converter, the power flowing into R can be used for useful purposes. In this case, the overall efficiency of the rectification circuit would increase significantly.

D. Experimental Setup II: AC Power Bridge Rectifier

The second experiment involves the comparison of two 230 V_{RMS}, 50 Hz bridge rectifiers with an average power of 445 W on a purely resistive load. One of the two circuits is built using diode-connected BJTs (see Fig. 6), while the other is based on saturated BJTs (see Fig. 7).

The two circuits under investigation are sized to work with a voltage source of peak amplitude $V_G = 325$ V (230 V_{RMS}), with $Rload \cong 119\ \Omega$, and with average power of 445 W and peak power of about 890 W. At this voltage and power level, the reverse bias junctions are subjected to a reverse bias peak voltage of about 325 V, while the peak current reaches about 2.72 A. The two circuits were built using the BJT BUL743 [26].

Since this power transistor, like other off-the-shelf BJT, cannot withstand a BE reverse voltage greater than a few volts, the roles of emitter and collector were swapped, according to the previous discussion and Fig. 5. In this way, the BUL743 operates by sustaining the reverse voltage on the BC junction. As a trade-off for the inversion between collector and emitter, the current gain i_E/i_B (please keep in mind that here the currents i_E and i_C are swapped compared to normal use) is quite low, but still sufficient for an evaluation of the benefits of the proposed configuration.

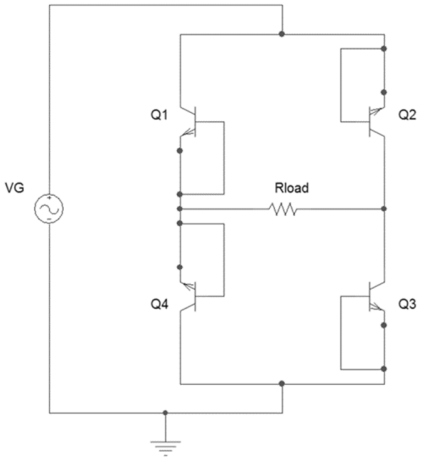

Fig. 6. Schematics of the bridge rectifier built with diode-connected inverted BJTs.

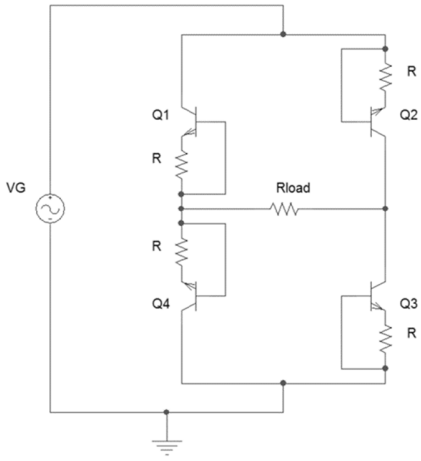

Fig. 7. Schematics of the bridge rectifier built with saturated inverted BJTs.

In the second circuit, shown in Fig. 7, a resistor R with a value of 0.5 Ω, was connected between the base and the emitter of the BUL743 BJT. The resistor value was experimentally selected to bias the BJT in saturation at the designed voltage and current levels. Experimental voltages were acquired by using a Tektronix MSO 2024B digital oscilloscope, while the currents were acquired using a LeCroy WaveSurfer 454 digital oscilloscope together with its current probe LeCroy AP015.

E. Experimental Setup II: Results

The voltages and currents of the transistor $Q1$ were measured in both circuits, and the power dissipated in the

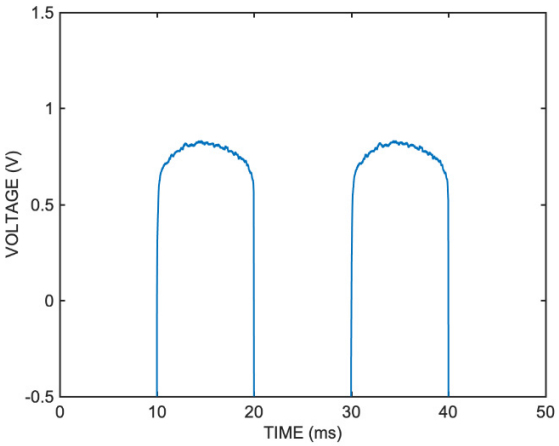

Fig. 8. Voltage v_{BC} in the diode-connected BJT $Q1$, where v_{EC} is equal to v_{BC} and $v_{BE} = 0$ due to the diode connection.

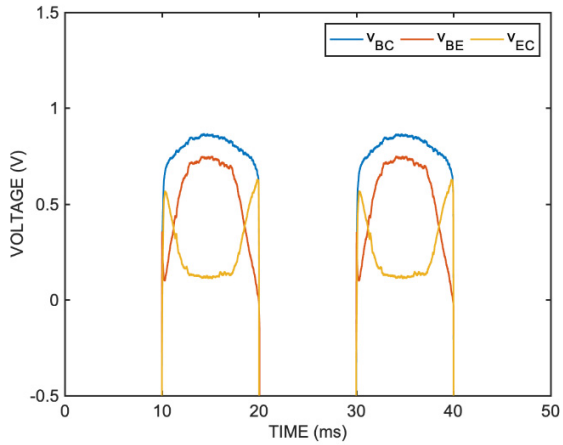

Fig. 9. Voltages in the saturated BJT $Q1$: v_{BC} (blue), v_{BE} (red), and v_{EC} (yellow).

transistors and in the resistor R was calculated from those measurements.

In Fig. 8, the voltage v_{BC} in the diode-connected BJT $Q1$ is shown. Due to the diode connection, $v_{EC} = v_{BC}$ and $v_{BE} = 0$. The peak value of v_{BC} is about 0.82 V, as expected for a diode-connected BJT that is always operating in the active region, reaching the value of a well forward-biased silicon diode.

Fig. 9 shows the three voltages v_{EC}, v_{BC}, and v_{BE}, for the saturated BJT $Q1$, with the relation $v_{BC} - v_{BE} = v_{EC}$. The peak value of v_{BC}, as expected for a saturated BJT, reaches that of a deeply forward-biased silicon diode, i.e., about 0.86 V. At the same time, the *EC* voltage level drops down to 0.12 V, due to saturation.

Figs. 10 and 11 show the currents i_B, i_E, and i_C in the two BJTs. Keep in mind that since the roles of the emitter and collector are swapped in our circuits, here $i_C = i_B + i_E$.

While in both transistors the i_C currents are very similar ($\approx$2.7 A peak) as expected, the current gains are however different. In the diode-connected BJT $Q1$ in Fig. 10, the current gain i_E/i_B is about 2.25, whereas, in the saturated BJT $Q1$ in Fig. 11, the current gain i_E/i_B is slightly more than 1, due to the deep saturation imposed by the presence of resistor R.

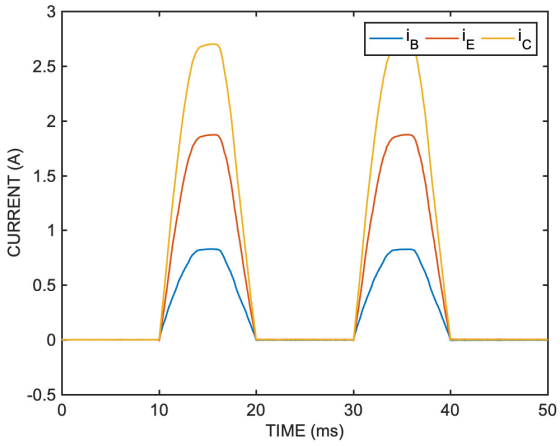

Fig. 10. Currents in the diode-connected BJT $Q1$: i_B (blue), i_E (red), and i_C (yellow).

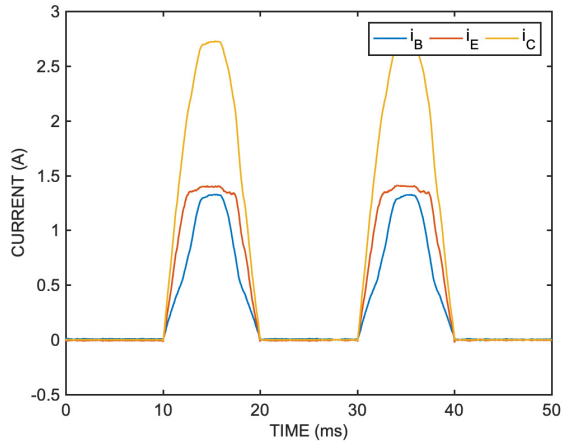

Fig. 11. Currents in the saturated BJT $Q1$: i_B (blue), i_E (red), and i_C (yellow).

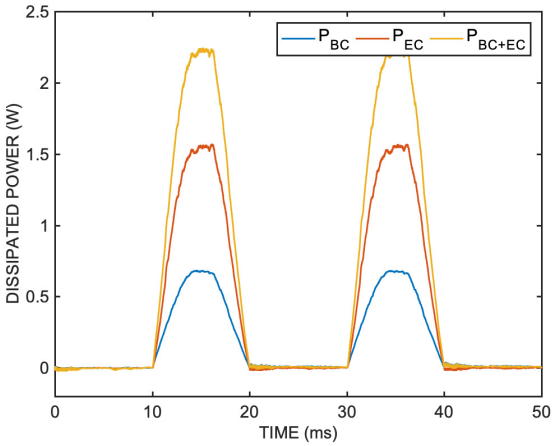

Fig. 12. Instantaneous dissipated power in the diode-connected BJT $Q1$: dissipated power in the *BC* terminals (blue), dissipated power in the *EC* terminals (red), and total dissipated power (yellow).

In Fig. 12, the instantaneous dissipated power in the diode-connected BJT $Q1$ is shown. The instantaneous power P_{BC} dissipated in the *BC* terminals is given by $i_B \cdot v_{BC}$ and the instantaneous power P_{EC} in the *EC* terminals is given by $i_E \cdot v_{EC}$. The total instantaneous dissipated power P_{BC+EC} is the sum of these powers, with a peak value of 2.23 W.

Fig. 13 shows the instantaneous dissipated power in the saturated BJT $Q1$. The power dissipated in the *BC* terminals

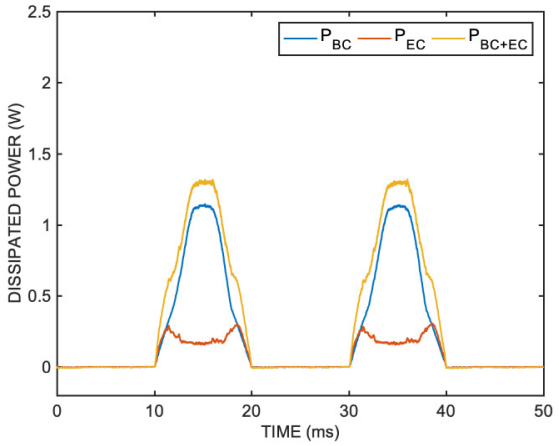

Fig. 13. Instantaneous dissipated power in the saturated BJT $Q1$: dissipated power in the BC terminals (blue), dissipated power in the EC terminals (red), and total dissipated power in the BJT (yellow).

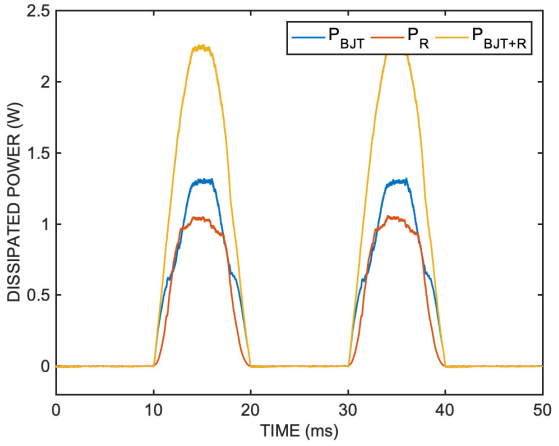

Fig. 14. Instantaneous dissipated power in the saturated configuration: dissipated power in the BJT (blue), dissipated power in R (red), and total dissipated power in the BJT plus R (yellow).

is given by $i_B \cdot v_{BC}$ and the power in the EC terminals is given by $i_E \cdot v_{EC}$. The total instantaneous dissipated power P_{BC+EC} is the sum of these powers.

Fig. 14 shows the total instantaneous dissipated power in the saturated BJT Q1, with a peak value of 1.22 W, the instantaneous dissipated power P_R in the resistor R, with a peak value of about 1 W, given by $i_E \cdot v_R = i_E \cdot v_{BE}$, and their summation $P_{\text{BJT}+R}$, with a peak value of 2.24 W.

F. Experimental Setup II: Discussion

The experimental results show that the proposed rectification scheme also works in ac, and with a transistor, the BUL743, which has characteristics not ideally suited for this purpose, as mentioned above. In fact, its reverse current gain β_{REVERSE} is less than 2.5 in the active region and approaches 1 in saturation. Despite this, the advantage of reducing the power dissipated in the semiconductor element is clearly visible.

In fact, the total instantaneous power dissipated in the rectifying element ($Q1$ in the circuit of Fig. 6 and $Q1 + R$ in the circuit of Fig. 7) is practically the same, as is evident from comparing Figs. 12 and 14, indicating that the efficiency is essentially the same for both circuits.

However, a significant difference in the power dissipated in the two BJTs can be seen by comparing Figs. 12 and 13. The diode-connected BJT dissipates a peak power of 2.23 W, while the saturated BJT dissipates a peak power of 1.22 W, with a reduction of about 45.3% of the dissipated peak power. The difference of about 1 W between the two peak powers is dissipated in the resistor R.

IV. Conclusion

A novel biasing scheme for current rectification using BJT was presented. The BJT is deeply saturated and its power dissipation is small compared to traditional diode and diode-connected BJT designs. Most of the power involved in the rectification process is dissipated in the external resistance R, which can advantageously be made to operate at very high temperatures and placed at an appropriate distance from the BJT. Reducing the power dissipated in the BJT is essential for reducing its temperature and obtaining a long operating life. The power balances of the three circuits were explained using basic voltage–current BJT relationships, which showed that, under reasonable assumptions, in the proposed circuit the power dissipation is largely transferred from the BJT to the external resistor R.

Three current rectifier schemes were built and experimentally compared, with a total power of approximately 10 W for each circuit. The measurements showed that the power dissipated in the BJT of the proposed circuit was 17 times lower than that measured in the diode (respectively 13.2 versus 231.9 mW), under the same operating conditions and with a similar level of overall maximum efficiency. Considerations of the physics acting on the semiconductor plausibly explain the calculated and observed power balance, considering that the heat released in one junction is almost entirely absorbed in the other.

A second set of experiments was conducted on a bridge rectifier with an input voltage of 230 V_{RMS}, a power output of approximately 445 W, and a resistive load. Even when employing a power BJT, the BUL743, which is not ideally suited for the proposed configuration due to its characteristics, a significant reduction in dissipated peak power (−45.3%) was observed compared to employing the same BJT in a diode-connected configuration.

The reported results are notable from two points of view: 1) a thermal effect acting in the saturated BJT was highlighted and 2) a practical bias scheme was proposed and experimentally demonstrated using a saturated BJT in power current rectifiers, resulting in reduced heat release in the silicon device.

Moreover, it is important to note that reducing the thermal stress can significantly extend the MTBF, that is, the lifetime, of the proposed rectifier.

After further understanding and development, the proposed new saturated BJT design could find broad future applications in the ac–dc power conversion required, for example, in electric vehicle chargers and inverter-type air conditioners.

References

[1] G. Seguier, *Power Electronic Converters AC/DC Conversion*. New York, NY, USA: McGraw-Hill, 1986.

[2] P. T. Krein, *Elements of Power Electronics*. London, U.K.: Oxford Univ. Press, 1998.
[3] J. G. Kassakian, M. F. Schecht, and G. C. Verghese, *Principles of Power Electronics*. Reading, MA, USA: Addison-Wesley, 1991.
[4] M. H. Rashid, *Power Electronics: Circuits, Devices, and Applications*, 2nd ed. Upper Saddle River, NJ, USA: Prentice-Hall, 1993.
[5] J. P. Agarwal, *Power Electronics Systems: Theory and Design*. Upper Saddle River, NJ, USA: Prentice-Hall, 2001.
[6] B. Singh, B. N. Singh, A. Chandra, K. Al-Haddad, A. Pandey, and D. P. Kothari, "A review of single-phase improved power quality AC–DC converters," *IEEE Trans. Ind. Electron.*, vol. 50, no. 5, pp. 962–981, Oct. 2003, doi: 10.1109/TIE.2003.817609.
[7] B. Singh, S. Gairola, B. N. Singh, A. Chandra, and K. Al-Haddad, "Multipulse AC–DC converters for improving power quality: A review," *IEEE Trans. Power Electron.*, vol. 23, no. 1, pp. 260–281, Jan. 2008, doi: 10.1109/TPEL.2007.911880.
[8] K. Ohyama and T. Kondo, "Energy-saving technologies for inverter air conditioners," *IEEJ Trans. Electr. Electron. Eng.*, vol. 3, no. 2, pp. 183–189, Mar. 2008, doi: 10.1002/TEE.20254.
[9] T. Endo et al., "Power electronics technology applied in inverter air conditioners," in *Proc. 23rd Int. Conf. Electr. Mach. Syst. (ICEMS)*, Nov. 2020, pp. 2095–2100, doi: 10.23919/ICEMS50442.2020.9290812.
[10] L. Shi, A. Meintz, and M. Ferdowsi, "Single-phase bidirectional AC–DC converters for plug-in hybrid electric vehicle applications," in *Proc. IEEE Vehicle Power Propuls. Conf.*, Sep. 2008, pp. 1–5, doi: 10.1109/VPPC.2008.4677506.
[11] Y.-J. Lee, A. Khaligh, and A. Emadi, "Advanced integrated bidirectional AC/DC and DC/DC converter for plug-in hybrid electric vehicles," *IEEE Trans. Veh. Technol.*, vol. 58, no. 8, pp. 3970–3980, Oct. 2009, doi: 10.1109/TVT.2009.2028070.
[12] A. Affam, Y. M. Buswig, A.-K.-B. H. Othman, N. B. Julai, and O. Qays, "A review of multiple input DC–DC converter topologies linked with hybrid electric vehicles and renewable energy systems," *Renew. Sustain. Energy Rev.*, vol. 135, Jan. 2021, Art. no. 110186, doi: 10.1016/j.rser.2020.110186.
[13] A. Khosroshahi, M. Abapour, and M. Sabahi, "Reliability evaluation of conventional and interleaved DC–DC boost converters," *IEEE Trans. Power Electron.*, vol. 30, no. 10, pp. 5821–5828, Oct. 2015, doi: 10.1109/TPEL.2014.2380829.
[14] J. Taufiq, "Power electronics technologies for railway vehicles," in *Proc. Power Convers. Conf.*, Nagoya, Japan, Apr. 2007, pp. 1388–1393, doi: 10.1109/PCCON.2007.373146.
[15] F. Blaabjerg, K. Ma, and D. Zhou, "Power electronics and reliability in renewable energy systems," in *Proc. IEEE Int. Symp. Ind. Electron.*, May 2012, pp. 19–30, doi: 10.1109/ISIE.2012.6237053.
[16] A. Sewergin, A. Stippich, and A. H. W. R. W. De Doncker, "Comparison of high performance cooling concepts for SiC power modules," in *Proc. IEEE Appl. Power Electron. Conf. Expos. (APEC)*, Mar. 2019, pp. 2822–2825, doi: 10.1109/APEC.2019.8722147.
[17] J. Bardeen and W. H. Brattain, "The transistor, a semi-conductor triode," *Phys. Rev.*, vol. 74, no. 2, pp. 230–231, Jul. 1948.
[18] W. Shockley, "Circuit element utilizing semiconductive material," U.S. Patent 2 569 347, Sep. 15, 1951.
[19] S. M. Sze and K. K. Ng, *Physics of Semiconductor Devices*. Hoboken, NJ, USA: Wiley, 2006.
[20] J. J. Ebers and J. L. Moll, "Large-signal behaviour of junction transistors," *Proc. Inst. Radio Eng.*, vol. 42, pp. 1761–1772, Dec. 1954.
[21] W. Thomson, "On a mechanical theory of thermoelectric currents," in *Proc. Roy. Soc.*, Edinburgh, Scotland, 1851, pp. 91–98.
[22] Y. G. Gurevich and I. Lashkevych, "Sources of fluxes of energy, heat, and diffusion heat in a bipolar semiconductor: Influence of nonequilibrium charge carriers," *Int. J. Thermophys.*, vol. 34, no. 2, pp. 341–349, Feb. 2013, doi: 10.1007/s10765-013-1416-0.
[23] O. Y. Titov, J. E. Velazquez-Perez, and Y. G. Gurevich, "Mechanisms of the thermal electromotive force, heating and cooling in semiconductor structures," *Int. J. Thermal Sci.*, vol. 92, pp. 44–49, Jun. 2015, doi: 10.1016/j.ijthermalsci.2015.01.023.
[24] Datasheet. (2024). *ON SEMICONDUCTORS 2SC6082*. Accessed: May 5, 2024. [Online]. Available: https://www.onsemi.com/download/data-sheet/pdf/2sc6082-d.pdf
[25] Datasheet. (2024). *VISHAY VS-20ETS16THM3*. Accessed: May 5, 2024. [Online]. Available: https://www.vishay.com/docs/96536/vs-20ets16thm3.pdf
[26] Datasheet. (2024). *STMicroelectronics BUL743 High Voltage Fast-Switching NPN Power Transistor*. Accessed: May 5, 2024. [Online]. Available: https://www.st.com/resource/en/datasheet/bul743.pdf

Riccardo Carotenuto (Senior Member, IEEE) was born in Rome, Italy. He received the Dr. Sc. degree in electronic engineering and the Ph.D. degree from the University "La Sapienza" of Rome, Rome, in 1992 and 1997, respectively.

He has been an Associate Professor of Electronics with the Mediterranea University of Reggio Calabria, Reggio Calabria, Italy, since 2002. He authored or co-authored more than 130 papers published on International Journals and Conferences Proceedings. His research interests include power conversion, energy harvesting, indoor localization, ultrasound imaging, ultrasound actuators, neural networks theory, and applications.

Demetrio Iero was born in Reggio Calabria, Italy, in 1982. He received the master's degree in electronic engineering and the Ph.D. degree from the Mediterranea University of Reggio Calabria, Reggio Calabria, Italy, in 2010 and 2014.

He is currently a temporary Researcher with the DIIES Department, Mediterranea University of Reggio Calabria. His research interests include power electronics and switching power loss measurement, microcontrollers, the IoT, and RFID platforms.

Fortunato Pezzimenti received the Laurea and Ph.D. degrees in electronic engineering from the Mediterranea University of Reggio Calabria, Reggio Calabria, Italy, in 2000 and 2004, respectively.

He is currently an Associate Professor of electronics with the Mediterranea University of Reggio Calabria. His current research interests include design, modeling, and electrical characterization of wide bandgap semiconductor devices for high power, high frequency, and high temperature applications.

Francesco G. Della Corte (Senior Member, IEEE) was born in Naples, Italy. He received the M.S. degree in electronic engineering from the Università di Napoli Federico II, Naples, in 1988.

He was with Sirti Spa, CNR-IMM, ENEA, Optel-InP, and a Full Professor of electronics with the Mediterranea University of Reggio Calabria, Reggio Calabria, Italy. He is currently a Full Professor of electronics at the Università di Napoli Federico II. His research interests include integrated sensors, wide bandgap semiconductor device modeling, and silicon photonics, subjects on which he authored or coauthored more than 130 journal articles and holds three patents.

Massimo Merenda (Member, IEEE) received the bachelor's, master's, and Ph.D. degrees in electronic engineering from the Mediterranea University of Reggio Calabria, Reggio Calabria, Italy, in 2002, 2005, and 2009, respectively.

From 2003 to 2005, he was a fellow with the Institute of Microelectronics and Microsystems of the National Research Council (IMM-CNR), Naples, Italy. From 2011 to 2018, he was a Post-Doctoral Researcher with UNIRC. He was a Researcher with the Mediterranea University of Reggio Calabria and CNIT, from 2018 to 2021. He is currently a Senior Researcher at the DIIES Department of UNIRC and CNIT since 2022. His research interests include the design of CMOS integrated circuits, RFID, silicon sensors, embedded systems, energy harvesting, and the Internet of Things (IoT). He is currently working in the research field of edge computing for applications of the Internet of Conscious Things and beyond.

Open Access funding provided by 'Univ Mediterranea di Reggio Calabria' within the CRUI CARE Agreement